Investigations of physical processes in the corona of laser-fired shell targets

Yu. V. Afanas'ev, N. G. Basov, B. L. Vasin, P. P. Volosevich, E. G. Gamaliĭ, S. Yu. Gus'kov, N. N. Demchenko, Yu. A. Zakharenkov, N. N. Zorev, A. A. Kologrivov, V. B. Rozanov, A. A. Rupasov, A. A. Samarskiĭ, G. V. Sklizkov, and A. S. Shikanov

P. N. Lebedev Physics Institute, USSR Academy of Sciences
(Submitted 30 March 1979)
Zh. Eksp. Teor. Fiz. 77, 2539–2554 (December 1979)

The interaction of nanosecond laser radiation with shell targets in the shell-compression regime and the formation and the corona state of a laser target are investigated. Experiments performed with the Kal'mar system yielded the absorbed, reflected, and refracted fractions of the laser radiation energy as well as the dependence of these quantities on the shell parameters. The temperature and density distributions of the plasma in the laser-target corona are measured. A theoretical analysis and numerical calculations indicate that the laser-radiation absorption is of inverse bremsstrahlung origin and that the fraction of the resonant absorption is small ($<1\%$). They demonstrate also the substantial role of the refraction in spherical experiments and the connection between the hydrodynamic processes in the target corona and the shell dynamics. The agreement between the experimental results and the numerical calculations makes it possible to conclude that the hydrodynamic model of the corona with classical inverse bremsstrahlung of the laser radiation and with Spitzer thermal conductivity is correct.

PACS numbers: 52.80.Hc, 52.50.Jm

I. INTRODUCTION

Most recent studies of laser-fired thermonuclear fusion[1] are devoted to theoretical and experimental studies of the heating and compression of spherical shell targets. In contrast to the concept of maximum isentropic compression of a homogeneous target by a laser pulse having specially profiled time waveform,[2] the suggestion of obtaining thermonuclear densities and temperatures by using shell targets having a definite internal structure but fired by a laser pulse having a relatively simple time waveform was advanced earlier.[3] At present it is precisely shell targets of various structures that are believed to be of possible use in the thermonuclear power reactors of the future, since the use of such targets at laser energies 10^5–10^6 J can lead[4] to an energy gain (ratio E_{TN}/E_L of thermonuclear and laser energies) on the order of several hundred. The greater part of the experiments on spherical heating and compression were therefore performed to data in various laboratories all over the world with thin-wall shell targets. A technology of producing and selecting targets in the form of thin-wall organic and glass shells was developed for these experiments, together with methods for filling them with hydrogen gas (or D_2 and DT gas) under pressure.[5,6]

Present-day experiments can be arbitrarily divided into two groups. The first includes experiments in which the laser-pulse is shorter than the shell-collapse time, and the radiation flux density is $q \gtrsim 10^{15}$ W/cm^2 (the Argus and Janus systems[7]). In these experiments the shell wall thickness was ~1 μm, and the shell was heated by a thermal wave even before the collapse, and its density became lower than the initial value (the so-called "exploding-shell" regime). The final gas and shell densities attained in this regime were small. However, the high thermal conductivity made the asymmetry of the irradiation and of the shell shape, as well the hydrodynamic instabilities of the compression, negligible in this regime.

In the second group of experiments the laser pulse duration was comparable with the shell collapse time, and moderate radiation intensities $q \sim 10^{14}$ W/cm^2 were used (the Kal'mar and C_6 systems).[8,9] In this case the internal part of the shell has not yet evaporated by the instant of maximum gas compression, and its density can exceed substantially the initial value (the "compressed-shell" regime). An important feature of this regime is that the initial entropy is fed into the compressed thermonuclear matter only by the shock wave, and this entropy turns out to be considerably lower than in the exploding-shell regime, when entropy is additionally supplied by fast electrons. As a result, the compressions attained in the compressed-shell regime are much higher ($\delta \sim 10^3$) at lower gas temperatures ($T \sim 0.2$–0.5 keV) than in the exploding-shell regime, in which these parameters are respectively $\delta \sim 10^2$ and $T \sim 3$–7 keV.

Theoretical investigations have shown[10] that in the compressed-shell regime it is possible to attain the thermonuclear-matter densities needed for thermonuclear fusion, even at the energy levels of contemporary lasers (10^2–10^3 J) if definite requirements are met with respect to the irradiation symmetry and the target shape, and it is precisely in this regime that experiments are feasible with positive energy yield, since the high value of the parameter ρR ($\rho R \gtrsim 0.1$ g/cm^2) can lead to the development of a thermonuclear-combustion wave.[11] In this paper we discuss the results of experimental investigations with the Kal'mar system and a theoretical analysis of the interaction of nanosecond laser radiation with shell targets and of the processes in the corona of laser targets. These include the absorption and refraction of the laser radiation, the heating and ionization of the corona material, and the shaping of its density profile. The dynamics of the target compression and the heating of the thermonuclear fuel in the compressed-shell regime are the subject of another study.[12]

 0038-5646/79/121229-09$02.40

II. EXPERIMENTAL SETUP

We present results of investigations performed on the nine-channel "Kal'mar" laser system. This system is described in detail in the literature (see, e.g., Refs. 13 and 14); we consider only the conditions of the laser-beam focusing on the target and list the employed diagnostic methods. The laser energy at the output of the system reached values $E_L \approx 150$ J at a pulse duration 150 nsec at the base and at a rise time $\tau_f \lesssim 0.5$ nsec while the half-width of the emission line was $\Delta\lambda \lesssim 10$ Å.[14] The nine laser beams were focused from different directions onto the target with the aid of independent two-lens systems with effective length $F \approx 20$ cm. The focal plane of each of the focusing systems was somewhat farther than the target, and the distribution of the laser-emission intensity near the target is approximated satisfactorily by the expression.

$$I(\xi) = I_0 \exp\{-(\xi/a)^2\} + I_1, \qquad (1)$$

$0 \leqslant \xi \leqslant 350$ μm, $a = 70$ μm, $I_1/I_0 = 1.72 \times 10^{-2}$, with ξ the distance to the optical axis. The first term in (1) describes the part of the laser radiation with the small divergence angle ($\alpha < 2 \times 10^{-4}$ rad), and the second corresponds to the distribution wings, whose existence is due to the presence in the heating beams of radiation with large divergence angle. At an energy ~100 J in the target region, the flux density at the maximum of the laser pulse was $q \approx 2 \times 10^{14}$ W/cm^2.

The targets used were hollow glass shells filled with deuterium gas, of diameter $2R_0 = 70 - 300$ μm and wall thickness $\Delta R = 0.5 - 4$ μm. The methods used to manufacture the shells, fill them with gas, and for selection and control were developed at our Institute.[5] The shell dimensions were monitored by interferometry. The target was suspended on a rubber-cement filament of thickness not larger than 0.5 μm stretched on a *U*-shaped holder.

We list now briefly the main diagonstic methods used in the experiments.

1. Measurement of the energy balance: 1) calorimetric measurements of the reflected and refracted radiation propagating past the target[15]; 2) measurements of the absorbed energy with the aid of open-type calorimeters[15]; 3) registration of the motion of the shock wave in the residual gas surrounding the target, using multiframe shadow and Schlieren photography.[16]

2. High-speed interferometry of the plasma corona: 1) with streak photography of the image in an electron-optical converter[17] 2) using frame-by-frame photography.[18]

3. Investigation of the space and time behavior of the luminous region of the plasma at the second harmonic frequency.[19]

4. Investigation of the contours of the spectral lines of the harmonics $2\omega_0$ and $(\frac{3}{2})\omega_0$: 1) with spatial resolution and integrated in time[20]; 2) streak photography with an image converter.[21]

5. Investigation of the plasma luminosity in the soft x-ray band using multichannel pinpoint cameras with high spatial resolution.

6. Registration of the spectral distribution of the continuous x radiation: 1) with x-ray films (1 keV $\lesssim h\nu \lesssim$ 10 keV)[22]; 2) with a scintillator and multipliers ($h\nu > 5$ keV).

7. Registration of neutron yield: 1) with integrating neutron-number counter; 2) time-of-flight neutron registration with scintillators and multipliers.

8. Investigation of the charge and energy makeup of the plasma particles[23]*:* 1) with ion collectors; 2) with a single-channel electrostatic mass spectrometer.

III. ABSORPTION OF LASER RADIATION AND FORMATION OF LASER-PLASMA CORONA

The laser radiation is absorbed in the target corona in the entire region whose density is lower than critical ($\omega = \omega_{cr}$) because of the inverse bremsstrahlung, and in a narrow region near the critical surface as a result of the anomalous (nonlinear) and resonance mechanisms. Resonant absorption is connected with the presence of a longitudinal (in the beam-incidence plane) component of the electric field in the light wave.[24]

An important role is played under conditions of spherical target irradiation by refraction of the laser radiation,[25] since some of the beams are deflected away from the beam axis and do not reach the region of most effective absorption near the critical surface. A theoretical investigation of the absorption and refraction of laser radiation in the plasma corona and a study of the role of various absorption mechanisms were carried out by numerical methods using the "Rapid" program, which comprises a combined system of Maxwell's equations and single-liquid two-temperature hydrodynamics with electronic heat conduction and ionic viscosity.[25] The distribution of the laser radiation intensity in the beam near the target were specified in the calculations in accord with Eq. (1).

The absorption of laser radiation by the target in the Kal'mar system was investigated experimentally by various methods, including two calorimetric procedures, measurements with ion collectors and with a mass spectrometer, and the method of a shock wave in the residual gas.

The first calorimetric method consisted of determining the absorbed energy E_{ab} by measuring the total laser energy entering the vacuum chamber (E_i) and the energy losses due to the refraction (E_r) and due to the presence of radiation with large divergence angle in the heating beams [see (1)] propagating past the target (E_t). The measurements were performed with an assembly of calorimetric sensors and recording apparatus developed at the Experimental Design Office of our Institute.[15] The arrangement of the sensors is shown schematically in Fig. 1. The Energy E_i was measured by calorimeters *3* in all the heating beams, with account taken with the losses in the deflecting and focusing optical systems, while the energy E_t was measured with calorimeters *4* in three out of the nine beams. The energy E_r of the refracted radiation was determined by averaging and recalculating to the total solid angle the readings of five

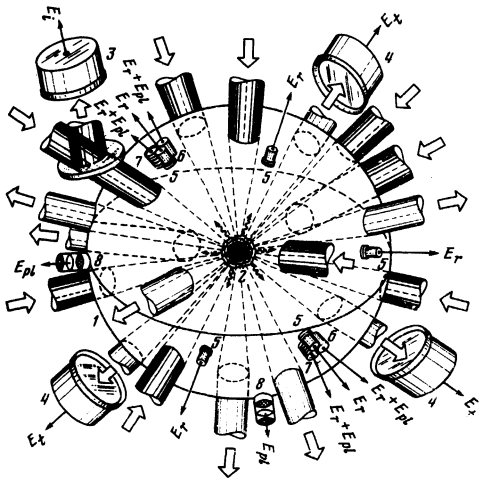

FIG. 1. Relative positions of the heating beams and the calorimetric sensors: 1—vacuum chamber, 2—target, 3, 4—KDS calorimeters, 5—VChDM calorimeters closed with filters, 6—open VChDM calorimeters, 7—open DG calorimeters, 8—electorstatic ion collectors; the arrows mark the heating beams and those propagating past the target.

VChDM miniaturized high-sensitivity sensors *5* covered with protecting glass and with light filters and placed at various points inside the vacuum chamber.

The second calorimetric method of determining the absorbed energy is similar to that used by Charatis *et al.*[26] It is based on a comparison of two closely placed sensors, one open and the other covered by protecting glass and light filters. The open VChDM sensor (*6*, Fig. 1) or a special open DG-1 sensor (*7*, Fig. 1) measures the total energy $E_{pl} + E_r$ of the expanding target material, of the radiation of the plasma proper, and of the radiation refracted in the plasma, while the closed sensors measure only the refracted energy E_r.

Figures 2 and 3 show the experimental and theoretical energy-balance components (calculated with the "Rapid" program without allowance for the anomalous absorption mechanisms), normalized to the laser energy entering the vacuum chamber, as functions of the target diameter. The increase in the spread of the experimental values of the energy past the target (Fig. 2a) with decreasing diameter is apparently due to the some inaccuracy in the aiming of the optical axes of the heating beam onto the center of the target. The relative contribution of this effect to the measurement error increases with decreasing target dimensions. Since the numerical simulation was based on the assumption that all the optical axes passed through the target center, the calculated plot lies in the lower part of the experimental-value band. The fraction of the refracted energy is 30–40% (Fig. 2). The difference between the readings of each of the five calorimeteric sensors, which characterizes the degree of asymmetry of the angular distribution of the refracted radiation from all the laser beams, did not exceed 40%.

The fraction of energy absorbed by the plasma, determined by the first calorimetric method, increases from ~15 to 50% with increasing shell diameter from 80 to 260 μm (Fig. 3). One of the causes of the differences

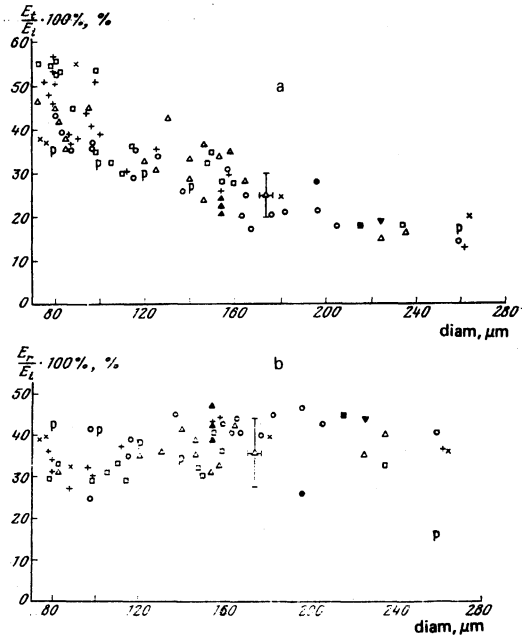

FIG. 2. Plots of energy moving past the plasma (a) and of the refracted energy (b), normalized to the lazer radiation energy entering the vacuum chanber, E_i, against the target diameter: $0.5 \leqslant \times < 0.9$ μm, $0.9 \leqslant + < 1.25$ μm, $1.25 \leqslant \square < 1.65$ μm, $1.65 \leqslant \Delta < 2.25$ μm, $2.25 \leqslant \circ < 3$ μm. *P*—calculated values for shells 2.2 μm thick.

between the theoretical and experimental values of the refracted and absorbed energy at large diameters (200–260 μm) may be the loss of spherical symmetry of the target irradiation, meaning also of the hydrodynamic character of the corona expansion in the case when the shell dimension exceeds substantially the diameter of the heating beams (see also Ref. 27).

In addition, numerical calculations show that at larger target diameters an increase takes place in the solid angle of the cone behind the target, which does not receive the radiation refracted by each of the heating beams. This increases also the asymmetry of the resultant distribution of the refracted radiation and possibly increases the inaccuracy in the determination of E_r.

An analysis of the results of the numerical calculation shows that under the conditions of the experiments with the Kal'mar system the contribution of the resonant absorption mechanism is small and amounts to ~1% of the

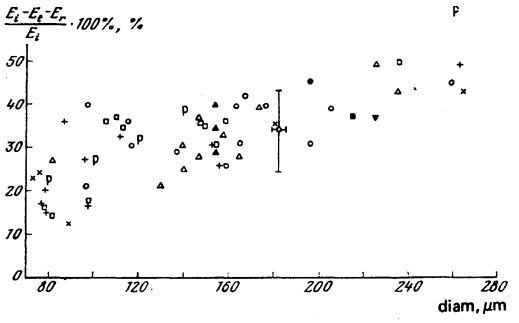

FIG. 3. Energy absorbed by plasma, normalized to the energy E_i, vs. the target diameter. The symbols are the same as in Fig. 2.

absorbed energy. This is due, first, to the features of the focusing system and, second, to the fact that in the regime wherein the shell is compressed a corona with a small density gradient is produced if the pulse duration is long enough, so that for most beams the distance from the turning point to the critical point exceeds substantially the radiation wavelength. The typical density profile in the corona is close to exponential, and the density decreases by a factor e at a distance ≈ 30 μm from the critical surface.

We note that when the flux density of the laser radiation on the target is increased the ponderomotive forces, which are capable of deforming the plasma profile near the critical density, assume a greater role. Attwood *et al.*[28] registered this deformation in experiment. Figure 4 shows the calculated plots of the fraction of the absorbed flux q_{abs}/q_{las} and of the relative contribution of the resonant absorption q_{abs}^{res}/q_{abs} against the density discontinuity $\Delta\rho/\rho_{cr} = (\rho_2 - \rho_1)/\rho_{cr}$ near the critical surface. The plasma profile was modified in such a way that the density varied in the range $\rho_1 \leqslant \rho \leqslant \rho_2$ over a distance 1 μm. It follows also from the calculations that the characteristic values of the ratio of the light pressure $p_l = |E|^2/16\pi$ to the thermal pressure $p_t = n_e T_e + n_i T_i$ amounts to 0.01–0.02, and according to Kidder's formula[29] the density discontinuity is $\Delta\rho/\rho_{cr} \approx (p_l/p_t)^{1/2} \sim 0.1$. It follows from Fig. 4 that the influence of this deformation on the absorption is negligible The role of the anomalous absorption mechanisms can also be regarded as negligible.

We do not have at present a complete physical picture of the anomalous absorption, and are therefore unable to speak of quantitative comparison. For example, allowance for the anomalous mechanisms obtained for a homogeneous quiescent plasma[30] leads to an increase of the fraction of the absorbed energy by a factor 1.5. Under the Kal'mar experimental conditions, owing to inhomogeneities of the plasma and of its motion, the instability-development pressures are apparently negligibly exceeded at $q < 10^{14}$ W/cm^2. It must therefore be assumed that practically the entire energy of the laser radiation is absorbed via the inverse-bremsstrahlung mechanism.

The results of the measurements of the adsorbed energy by the second calorimetric method agree well with

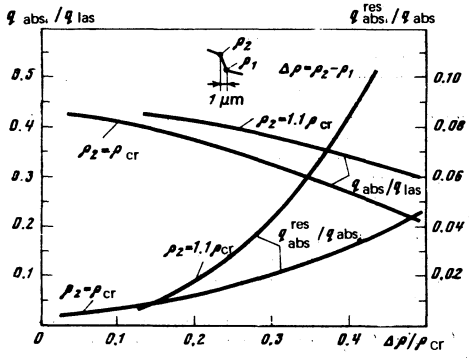

FIG. 4. Calculated dependence of the absorption coefficient and of the fraction of the resonantly absorbed energy on the discontinuity of the plasma density profile; $T_e = 0.6$ keV.

the measurements by the first method, An advantage of the second method is that placing the open calorimeter in the immediate vicinity of the closed one eliminates the influence of the anisotropy of the directivity pattern of the refracted radiation on the measurements of the absorbed energy. It must be noted, however, that this method, in contrast to the first, underestimates the absorbed energy in those experiments in which residual D_2 gas remains in the vacuum chamber and its pressure amounts to several torr. The reason is that the shock wave that propagates in the gas and carries part of the energy absorbed by the plasma has time to be transformed into a sound over the distance to the calorimeter location, and is no longer registered by them.

The energy absorbed by the plasma is converted into the energy of the spreading plasma particles and into electromagnetic radiation having an intensity maximum in the x-ray region. The energy of the soft x rays was estimated from measurements made with multichannel film detectors, and reached in individual flashes ~0.5 J (~2% of the absorbed energy). Measurement of the energy of the spreading plasma particles with mass spectrometers and ion collectors determines with sufficient accuracy the absorbed energy. The use of this method in our experiments yielded results close to those obtained by calorimetric measurements.

The last method of determining the absorbed energy consisted of measuring the energy of the spherical shock wave in the residual gas by obtaining the $R-t$ diagram of its motion using multiframe Schlieren photography.[16] We used for this purpose the equations that describe the propagation of a strong ionizing shock wave in a homogeneous atmosphere.[31] However, the values obtained by this method for the absorbed energy were always somewhat lower than the corresponding values obtained by the calorimetric measurements.

It must be noted that measurement of the energy absorbed by the plasma when spherical targets are fired by multichannel lasers is a most complicated tasks. In the case of calorimetric measurements, for example, the reason is the strong refraction of the heating radiation in the plasma corona, which leads to nonuniform scattering of the radiation (into a solid angle 4π sr) and measuring of this scattering is made most difficult by the large number of elements of the diagnostic appartus and of the focusing system in the vacuum chamber. Therefore only combined use of several procedures that record the energy balance components by different methods make it possible to determine the absorbed energy with sufficient accuracy.

2. Laser-target corona

The principal processes responsible for the formation of the laser-target corona are (besides the laser-radiation absorption considered briefly in the preceding section) ionization, energy transport by electronic thermal conductivity, relaxation between the electronic and ionic components of the plasma, spreading of the material, and x radiation. We discuss now in greater detail these processes and their mathematical description in the "Luch" program.[32]

The kinetics of the ionization of the plasma target is described in the program by the equation

$$d\bar{z}/dt=\bar{z}(\nu_e-\nu_{p.r.}-\nu_{t.r.}),\quad \bar{z}>1, \tag{2}$$

in which the respective rates ν_e, $\nu_{p.r.}$, and $\nu_{t.r.}$ of ionization by electron impact, of photorecombination, and of triple recombination were taken from the paper of Beĭgman *et al.*[33] The disequilibrium of the ionization kinetics can cause the average ionization multiplicities at a given instant of time to differ by a factor of two from the equilibrium value. In the dense unevaporated part of the target, the plasma ionization takes place under equilbrium conditions. In the corona, at densities $n_e \sim n_{cr}$ and temperatures $T_e > 0.1$ keV the triple recombination rate $\nu_{t.r.}$ is much less than ν_e or $\nu_{p.r.}$ and in the equilibrium case we find from (2) that corona equilibrium occurs at $\nu_e = \nu_{p.r.}$. In the dense unevaporated part of the shell at $n_e \gtrsim 10^{22}$ cm^{-3} and $T_e \lesssim 0.02$ keV we have $\nu_{p.r} \ll \nu_e$, $\nu_{p.r.} \ll \nu_{t.r.}$, and the Saha equilibrium $\nu_e = \nu_{t.r.}$ is obtained.

Calculation of the ionization multiplicity is important also for the calculation of the x radiation from the corona. The energy equation contains the energy of the ionization in the corona. The influence of this effect can be observed by comparing the effective adiabatic exponent

$$\gamma_{eff}=1+\frac{p}{\varepsilon}=1+\frac{nkT}{{}^3/_2 nkT+Q(\bar{z})}$$

with $\gamma=\frac{5}{3}$. Thus, for the corona of a glass target ($T_e < 1$ keV) we have $\gamma_{eff} = 1.45$ to 1.5, which corresponds to an ionization energy $Q(\bar{z})$ amounting to 70–50% of the internal energy of the plasma $\varepsilon_{int} = (\frac{3}{2})nkT$. In the unevaporated part of the shell, account is taken of the cold pressure, whose role is significant.

The region where the laser radiation is absorbed is a source of electronic heat-conduction waves that transport energy both to the dense layers of the plasma and to the low-density expanding plasma. An analysis of experimental and theoretical investigations of the compression of glass shells shows that in the plasma produced by nanosecond laser pulses at flux densities $q \lesssim 10^{14}$ W/cm^2 there is no need to introduce the lowered (anomalous) thermal conductivity. The experiments[14] are satisfactorily described in the classical heat-conduction approximation. It follows from the numerical calculation that in the region where the thermal conductivity is significant we always have $l_e \ll L$ ($L = T_e/\nabla T_e$ and l is the electron mean free path), and consequently the classical (Spitzer) heat flux is substantially smaller than the maximum heat flux $n_e v_e k T_e$ carried by the particles without collisions, and is less than the flux corresponding to a transport velocity equal to the ion velocity v_i:

$$q_{Sp}=\varkappa_e \nabla T_e < n_e v_i k T_e \ll n_e v_e k T_e.$$

The relaxation processes in the corona and in the compressed part of the target differ in their character. At $\rho \gtrsim \rho_{cr}$ the laser energy is transferred in the corona mainly to electrons, and we always have $T_e > T_i$. In the compression region, where the energy is concentrated in the hydrodynamic motion, we have $T_i \gtrsim T_e$.

The x radiation is determined by the bremsstrahlung and recombination processes. The total radiation energy for the targets under consideration is less than 5% of the absorbed energy and does not influence the compression processes. There are in the target two regions that make the main contribution to the integrated luminosity: the corona region near the critical density, and the central part of the target, which is heated and compressed as a result of spherical cumulation. The maximum of the corona glow is shifted from the critical surface to the center of the target towards higher densities. The time of glow of this region is comparable with the duration of the laser pulse, and the spatial evolution is similar to the displacements of the critical surface. The time of glow of the central region of the target is 10^{-10}–10^{-11} sec. The main contribution is made by the emission of the heated glass layers adjacent to the gas. Since the thickness of these layers is small compared with the diameter of the compressed gas, and since the time variation of the size of the emitting region is slight, measurement of the size of the glowing region on the pinpoint photograph makes it possible to determine experimentally the volume compression of the gas.

The "Luch" program makes allowance for the volume x radiation. The x-ray transport was calculated by a special program in which the stationary transport equation was solved without allowance for the reaction of the radiation on the hydrodynamics. It is legitimate to use an approximation with a quasistationary radiation field corresponding to the instantaneous distribution of the absorption and emission sources, since the plasma velocity is much lower than that of light. The total emission of x rays from the target and its spectrum as well as the theoretical pinpoint pictures, were determined in the cited calculation by using the temperature and density distributions obtained in the "Luch" and "Rapid" calculations.

We proceed now to discuss the results of the experimental investigations of the laser-plasma corona. The space-time averaged electron temperatures of the plasma corona were determined from spectral measurements of the continuous x radiation by the absorber method. To register the x rays we used multichannel detectors whose sensitive element was the UF-VR x-ray film,[22] and a three-channel scintillation detector. The use of the latter was dictated by the desire to extend the recorded spectral range towards higher quantum energies.

Each of the registration channels of the scintillation detector consisted of a plastic scintillator covered by an absorber, a flexible light pipe, and a set of neutral light filters that set the required dynamic range of the measurement system. The signals from all three channels were registered with a common FÉU-30 photomultiplier and with a 6LOR-02 oscilloscope. In one detector channel we used a beryllium absorber 400 μm thick, and in the other two a combination of a beryllium filter of the same thickness with aluminum filters.

Figure 5 shows the results of measurements, made with a film detector on two shell targets, of the ratio of the number of photons passing through a beryllium filter of thickness δ_{Be} (which ranged from 500 to 2400 μm,

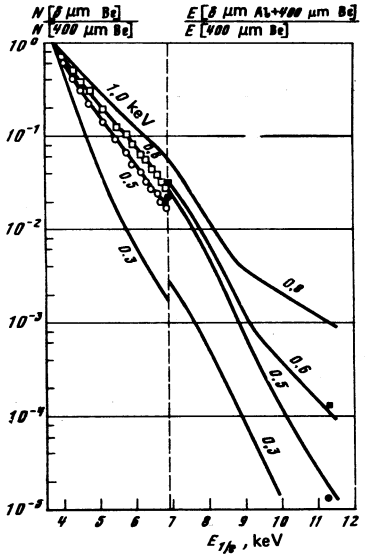

FIG. 5. Experimental and calculated ratios of the numbers of quanta and energies of the x radiation passing through filters of various thicknesses against the end-point cutoff energy of the filters. Target parameters: ○, ●—$2R=236$ μm, $\Delta R=1.7$ μm, □, ■—$2R=165$ μm, $\Delta R=2$ μm.

corresponding to end-point cutoff energies $E_{1/e}=3.7$–6.9 keV), to the number of photons passing through a 400-μm beryllium filter. The same figure shows for the range $E_{1/e}=6.9$–11.3 keV, the results of measurement, with a scintillation detector, of the ratio of the energy of the x rays passing through a combination of a 400-μm beryllium filter and an aluminium filter of thickness $\delta_{Al}=40$–200 μm, to the radiation energy passing through a 400-μm beryllium filter. The solid lines in the figures are the theoretical plots calculated for various electron temperatures, assuming a Maxwellian distribution of the plasma-electron velocities. Comparison of the experimental and calculated results shows that in the range of the end-point energies $E_{1/e}=3.7$–11.3 keV there is no substantial deviation of the plasma-electron distribution from Maxwellian, and the resultant values of the electron temperature in these two experiments is ~0.5 and 0.6 keV.

Generalization of the measurement results obtained in a large number of experiments shows that the space-time integrated values of the plasma electron temperatures in different shell targets lie in the range 0.3–0.9 keV.

To ensure the required time resolution in the measurement of the electron temperature in the plasma corona, a study was made of the temporal evolution of the spectral distribution of the $(\frac{3}{2})\omega_0$ harmonic generated in the plasma in the region of one-fourth the critical density $n_{cr}/4$. Experimental and theoretical investigations[34] have shown that the spectrum of the $(\frac{3}{2})\omega_0$ harmonic consists of two components that are shifted in opposite direction relative to the exact value $(\frac{3}{2})\lambda_0$ and separated by a distance proportional to the plasma electron temperature in the region of one-quarter the critical density; this makes it possible to determine the evolution of the electron temperature in this region on the basis of the spectral and temporal investigations of the spectrum of the harmonic, in accord with the relation[21]

$$T_e(t)\approx 1.5\cdot 10^3\Delta\lambda_{3/2}(t)/\lambda_0,$$

where $\Delta\lambda_{3/2}$ is the distance between the spectral components of the harmonic, λ_0 is the laser-emission wavelength, and T_e is in keV.

For example, in one of the shell targets,[21] at instants of time 0.8, 1.5, and 2.3 nsec, the distance between the components of the harmonic was 38, 44, and 32 Å, corresponding to an electron temperature in the $n_{cr}/4$ region 570, 660, and 480 eV, respectively. We note that the plasma electron temperature averaged over the emission time of the $(\frac{3}{2})\omega_0$ harmonic and obtained by the method described above agrees sufficiently well with x-ray measurements. Calculations of the heating and compression of target by the "Luch" program give average corona temperatures 0.5–1 keV close to the experimental ones.

Figure 6 shows a diagram of the optical system used for the diagnostics of the laser-plasma corona. To determine the degree of spherical expansion we used multiframe interferometry.[18] Streak scanning of the interference patterns and of the plasma glow region were simultaneously obtained with an electron-optical recorder at the second harmonic of the heating radiation[19,35] (the scan pictures were separated on the photorecorder by introducing an optical delay).

The time evolution of the electron spatial distribution function $n_e(r)$ was investigated by reducing the displacement interference pattern scans. The use of a three-mirror displacement interferometer greatly extended the registered range of plasma electron densities, to $n_e\sim 10^{20}$ cm^{-3}. Usually, if an objective with sufficient angular aperture ($\gtrsim 10°$) is used in the interferometry system, the upper limit of the registered densities consists of a very dense assembly of interference fringes that cannot be spatially resolved by the optical system. In a displacement interferometer, by adjusting the transverse displacement, it is possible to suppress the condensation effect to a considerable degree, since the phase difference between the phases of the interfering beams that have passed through the plasma over the dis-

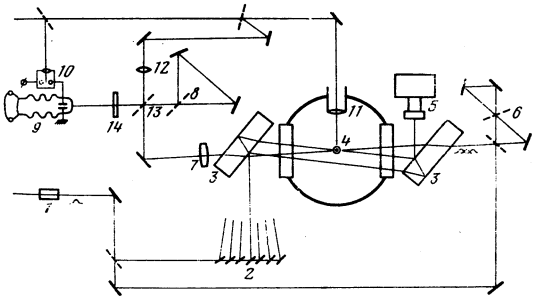

FIG. 6. Diagram of plasma optical-diagnostics system: 1—KDP crystal, 2—optical delay system, 3—Jamin interferometer, 4—target, 5—multiframe interference photographic camera, 6—system for the formation of the composite optical pulse, 7—objective, 8—displacement interferometer, 9—photoelectronic recorder, 10—laser triggered discharger, 11—lens to focus the heating radiation on the target, 12—lens, 13—semitransparent mirror, 14—interference light filter.

placement distance is much less (by a factor 2–3 in experiment) than in an ordinary two-beam interferometer. Among other advantages of the employed interferometer is also that only in a displacement interferometer it is possible to tune, in both directions from the target center, along the photorecorder slit, the optimal initial angle between the interfering beams,[17] when the fringes broaden in the denser regions of the plasma (Fig. 7).

Figure 8 shows the measured distribution $n_e(r)$ at various instants of time in two experiments, as well as the density profiles obtained in the numerical calculations of the same experiments in accord with the "Luch" program. An analysis the data shows not only a general agreement of the dynamics of the evolution of the calculated and experimental distribution, but also that their absolute values at the same point of space and at the same instant of time are close. This allows us to assume that the numerical calculation describes well the state of the laser-plasma corona and also such corona characteristics as the absorbed laser energy (see Sec. 1). The degree of ionization $\bar{z}$ and the evaporated mass are close to the calculated values. The calculations yielded $\bar{z} \sim 10$ and evaporated-mass values 30 and 40%, respectively. An interesting feature of the density distribution is that it reveals perturbations that are formed at the start of the second nanosecond. A theoretical analysis shows that this perturbation is produced by a shock wave that is reflected from the center, passes through the compressed part of the shell, and enters the corona. The time t_r of the registration of the perturbation at the point R_r consists of the time t^* of collapse of the shell (it can be approximately assumed that it is precisely at this instant that the shock wave from the deuterium enters into the compressed shell) and the times Δt_{sh} and Δt_c of propagation through the compressed shell and through the corona. Numerical calculation shows that in thin-wall shells $\Delta t_{sh} \approx 0.1 t^* \ll t^*$. The corona time is $\Delta t_c \approx R_r/\bar{w}$, where $\bar{w}$ is the average velocity of the perturbation after leaving the corona.

Thus, an investigation of the time evolution of the indicated density perturbations makes it possible to determine an important dynamic characteristic of the shell-target compression process, namely the collapse time: $t^* \approx t_r(R_r) - R_r/\bar{w}$.

Measurements of the positions of the perturbations at various instants of time yielded for the velocity $\bar{w}$ in the describes experiments values 8×10^7 and 5×10^7 cm/sec, hence $t^* = 1.4$ and 1.2 nsec. It must be noted that the problem of entry of the shock wave into the laser target corona is close to the known problem of the emergence of a shock wave on the surface of a star,[36] but its analytic solution is made difficult by the complicated character of the distribution of the temperature, density, and velocity of the matter in the plasma.

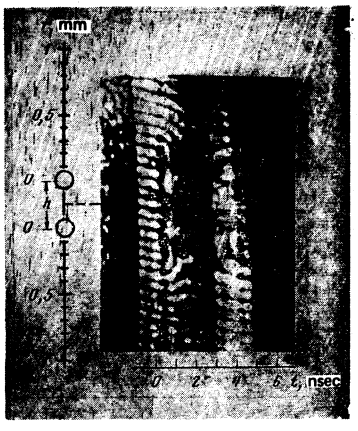

FIG. 7. Characteristic streak scan of displacement interference patterns of laser plasma. Lateral displacement $h \approx 400$ μm.

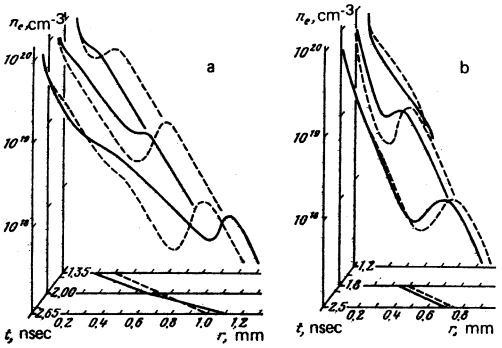

FIG. 8. Motion of shock wave in the plasma corona of a target. Solid lines—results of interferometry measurements; dashed-calculated profiles of electron density. a) diam 138 μm, Δ = 1.7 μm; b) diam 98 μm, Δ = 1.4 μm.

CONCLUSION

Our present results lead to the following conclusions concerning the formation and state of the corona of laser targets in Kal'mar experiments at moderate laser-radiation fluxes up to 10^{14} W/cm^2.

For shells of diameter $2R \approx 80$–100 μm the absorbed energy measured by various methods is ≈15–30% of the energy of the heating radiation, values close to those obtained in experiments[26,37,38] with analogous targets and with picosecond laser pulses, although these experiments were performed under better focusing conditions from the point of view of the diffraction losses. For larger shells, ≈200–250 μm in diameter, higher absorbed energy fractions, ≈50%, were registered. The investigations have demonstrated the important role of refraction in spherical irradiation: the fraction of the refracted energy was 30–40%. The measurement results agree sufficiently well with the results of numerical calculations based on the classical absorption model. The contribution of the resonance mechanism of absorption is small, and the fraction of the resonant absorbed energy is ~1%.

The space-time integrated plasma electron temperatures registered in the discussed experiments amount to ~0.3–0.9 keV for various shell targets. The use of classical Spitzer conductivity in the hydrodynamic model, at the indicated energy absorption, has made it possible, for both the theoretical analysis and the numerical calculation, to present a description of the state and dynamics of the laser-plasma corona in good agreement with experiment. This manifests itself clearly when the experimentally registered average temperature, and particularly the density profile of the corona, are compared with the experimental values.

[1]N. G. Basov and O. N. Krokhin, Zh. Eksp. Teor. Fiz. **46**, 171 (1964) [Sov. Phys. JETP **19**, 123 (1964)]; Vestnik Akad. Nauk SSSR No. 6, 55 (1972).
[2]J. Nuckolls, L. Wood, A. Thiessen, and G. Zimmerman, Nature **239**, 139 (1972).
[3]Yu. V. Afanas'ev, N. G. Basov, P. P. Volosevich, E. G. Gamaliĭ, O. N. Krokhin, S. P. Kurdyumov, E. I. Levanov, V. B. Rozanov, A. A. Samarskiĭ, and A. N. Tikhonov, Plasma Physics and Controlled Nuclear Fusion Research **2**, IAEA, Vienna, 1975, p. 559. J. Nuckolls, J. Lindl, W. Mead, A. Thiessen, L. Wood, and G. Zimmerman, Plasma Physics and Controlled Nuclear Fusion Research **2**, IAEA, Vienna, 1975, p. 535. G. S. Fraley, W. P. Gula, D. B. Henderson, R. L. McCrory, R. C. Malone, R. J. Mason, and K. L. Morse, Plasma Physics and Controlled Nuclear Fusion Research **2**, IAEA, Vienna, 1975, p. 543.
[4]Yu. V. Afanas'ev, N. G. Basov, P. P. Volosevich, E. G. Gamaliĭ, O. N. Krokhin, S. P. Kurdyumov, E. I. Levanov, V. B. Rozanov, A. A. Samarskiĭ, and A. N. Tikhonov, Pis'ma Zh. Eksp. Teor. Fiz. **21**, 150 (1975) [JETP Lett. **21**, 68 (1975)].
[5]E. G. Gamaliĭ, A. I. Gromov, A. I. Isakov, L. A. Krupinina, Yu. S. Leonov, F. I. Matveeva, Yu. A. Merkul'ev, A. I. Nikitenko, E. R. Rychkova, and G. V. Sklizkov, Tr. Fiz. Inst. Akad. Nauk **94**, 29 (1977).
[6]D. E. Solomon and T. M. Henderson, J. Appl. Phys. **8**, L85 (1975).
[7]Laser Program Annual Report, LLL, 1976.
[8]N. G. Basov, A. A. Kologrivov, O. N. Krokhin, A. A. Rupasov, G. V. Sklizkov, and A. S. Shikanov, Pis'ma Zh. Eksp. Teor. Fiz. **23**, 474 (1976) [JETP Lett. **23**, 428 (1976)]. N. G. Basov, Yu. A. Zakharenkov, N. N. Zorev, A. A. Kologrivov, O. N. Krokhin, A. A. Rupasov, G. V. Sklizkov, and A. S. Shikanov, Plasma Physics, Proc. of the Thirty Sixth Nobel Symposium, ed. by H. Wilhelmsson, Plenum Press, N. Y., 1977, p. 47. N. G. Basov, A. A. Kologrivov, O. N. Krokhin, A. A. Rupasov, G. V. Sklizkov, A. S. Shikanov, Yu. A. Zakharenkov, and N. N. Zorev, Laser Interactions and Related Plasma Phenomena, Proc. of the Fourth Workshop, Troy, 1976, ed. by H. Schwartz and H. Hora, Plenum Press, N. Y., Vol. 4A, 1977, p. 479.
[9]D. Billon, P. A. Holstein, J. Launspach, C. Patou, J. L. Rocchiccioli, and D. Schirmann, The Eleventh European Conf. on Laser Inter. with Matter, Abstracts reserved, IV, Oxford, 1977.
[10]Yu. V. Afanas'ev, H. G. Basov, P. P. Volosevich, E. G. Gamaliĭ, O. N. Krokhin, S. P. Kurdyumov, E. I. Levanov, V. B. Rozanov, A. A. Samarskiĭ, and A. N. Tikhonov, Kvantovaya Elektron. (Moscow) **2**, 1816 (1975) [Sov. J. Quantum Electron. **5**, 989 (1975)].
[11]K. A. Brueckner and S. Jorna, Rev. Mod. Phys. **46**, 325 (1974). S. Yu. Gus'kov, O. N. Krokhin, and V. B. Rozanov, Nucl. Fusion **16**, 6 (1976).
[12]N. G. Basov, P. P. Volosevich, E. G. Gamaliĭ, S. Yu. Gus'kov, A. A. Erokhin, Yu. A. Zakharenkov, N. N. Zorev, A. A. Kologrivov, V. B. Rozanov, A. A. Rupasov, A. A. Samarskiĭ, G. V. Sklizkov, and A. S. Shikanov, Zh. Eksp. Teor. Fiz. [Sov. Phys. JETP], in press.
[13]N. G. Basov. O. N. Krokhin, G. V. Sklizkov, S. I. Fedotov, and A. S. Shikanov, Zh. Eksp. Teor. Fiz. **62**, 203 (1972) [Sov. Phys. JETP **35**, 109 (1972)].
[14]N. G. Basov, Yu. A. Zakharenkov, N. N. Zorev, A. A. Kologrivov, O. N. Krokhin, A. A. Rupasov, G. V. Sklizkov, and A. S. Shikanov, Zh. Eksp. Teor. Fiz. **71**, 1788 (1976) [Sov. Phys. JETP **44**, 938 (1976)].
[15]B. L. Vasin, N. N. Zorev, V. N. Radaev, A. A. Rupasov, G. V. Sklizkov, A. S. Shikanov, and L. I. Shishkina, Preprint Fiz. Inst. Akad. Nauk SSSR, No. 198, 1978.
[16]A. A. Erokhin, Yu. A. Zakharenkov, N. N. Zorev, G. V. Sklizkov, and A. S. Shikanov, Fiz. Plazmy **4**, 648 (1978) [Sov. J. Plasma Phys. **4**, 362 (1978)].
[17]Yu. A. Zakharenkov, O. N. Krokhin, G. V. Sklizkov, and A. S. Shikanov, Kvantovaya Elektron. (Moscow) **3**, 1068 (1976) [Sov. J. Quantum. Electron. **6**, 571 (1976)].
[18]Yu. A. Zakharenkov, A. V. Rode, G. V. Sklizkov, S. I. Fedotov, and A. S. Shikanov, Kvantovaya Elektron. (Moscow) **4**, 815 (1977) [Sov. J. Quantum Electron. **7**, 453 (1977)].
[19]Yu. A. Zakharenkov, N. N. Zorev, O. N. Krokhin, Yu. A. Mikhaĭlov, A. A. Rupasov, G. V. Sklizkov, and A. S. Shikanov, Pis'ma Zh. Eksp. Teor. Fiz. **21**, 557 (1975) [JETP Lett. **21**, 259 (1975)].
[20]N. G. Basov, O. N. Krokhin, M. V. Osipov, A. A. Rupasov, V. P. Silin, G. V. Sklizkov, A. N. Starodub, V. T. Tikhonchuk, and A. S. Shikanov, Preprint Fiz. Inst. Akad. Nauk SSSR, No. 256, 1978.
[21]V. Yu. Bychenkov, Yu. A. Zakharenkov, O. N. Krokhin, A. A. Rupasov, V. P. Silin, G. V. Sklizkov, A. N. Starodub, V. T. Tikhonchuk, and A. S. Shikanov, Pis'ma Zh. Eksp. Teor. Fiz. **26**, 500 (1977) [JETP Lett. **26**, 364 (1977)].
[22]A. A. Kologrivov, Yu. A. Mikhaĭlov, G. V. Sklizkov, S. I. Fedotov, A. S. Shikanov, and M. R. Shpol'skiĭ, Kvantovaya Elektron. (Moscow) **2**, 2223 (1975) [Sov. J. Quantum Electron. **5**, 1210 (1975)].
[23]N. G. Basov, E. Volovski, E. Voryna, S. Denus, Yu. A. Zakharenkov, S. Kaliski, G. V. Sklizkov, Yu. Farny, and A. S. Shikanov, Preprint Fiz. Inst. Akad. Nauk SSSR, No. 194, 1978.
[24]V. L. Ginzburg, Rasprostranenie élektromagnitnykh voln v plazme (Propagation of Electromagnetic Waves in a Plasma), Nauka, 1967 [Pergamon].
[25]Yu. V. Afanasiev, N. G. Basov, E. G. Gamaly, V. A. Gasilov, N. N. Demchenko, O. N. Krokhin, T. G. Lebo, V. B. Rozanov, A. A. Samarsky, V. F. Tishkin, and A. P. Favorsky, Preprint Fiz. Inst. Akad. Nauk, 1977.
[26]G. Charatis, I. Downward, R. Goforth, *et al.*, Plasma Phys. and Controlled Nuclear Fusion Research, Proc. of the Intern. Conf. Tokyo, 1974; IAEA, Vienna, Vol. 2, 1975, p. 317.
[27]D. Billon, P. A. Holstein, J. Launspach, C. Patou, J. M. Reisse, and D. Schirmann, Laser Inter. and Related Plasma Phenomena, ed. by H. Schwarz and H. Hora, Plenum Press, N. Y., Vol 4A, 1977, p. 503.
[28]D. T. Attwood, D. W. Sweeney, I. M. Auerbach, and P. H. Y. Lee, Phys. Rev. Lett. **40**, 184 (1978).
[29]R. E. Kidder, Lawrence Livermore Lab. Report UCRL-74040. Russ. transl. in: Problemy lazernogo termoyadernogo sinteza (Problems of Laser Thermonuclear Fusion), Atomizdat, 1976, p. 135.
[30]V. P. Silin, Parametricheskoe vozdeĭstvie izlucheniya bol'shoĭ moshchnosti na plazmu (Parametric Action of High-Power Radiation on a Plasma), Nauka, 1973.
[31]N. N. Zorev, G. V. Sklizkov, and A. S. Shikanov, Investigation of Shock Waves Produced by Irradiation of Spherical Target by High-Power Laser Radiation, Paper at 12th European Conference on the Interaction of Laser Radaiation with Matter, Moscow, 1978.
[32]Yu. V. Afanas'ev, P. P. Volosevich, E. G. Gamaliĭ, O. N. Krokhin, S. P. Kurdyumov, E. I. Levanov, and V. B. Rozanov, Pis'ma Zh. Eksp. Teor. Fiz. **23**, 470 (1976) [JETP Lett. **23**, 425 (1976)]
[33]I. P. Beĭgman, L. A. Vainshteĭn, and A. V. Vinogradov, Astron. Zh. **46**, 985 (1969) [Sov. Astron. **13**, 775 (1970)]
[34]A. I. Avrov, V. Yu. Bychenkov, O. N. Krokhin, V. V. Pustovalov, A. A. Rupasov, V. P. Silin, G. V. Sklizkov, V. T. Tikhonchuk, and A. S. Shikanov, Pis'ma Zh. Eksp. Teor. Fiz. **24**, 293 (1976) [JETP Lett. **24**, 262 (1976)]; Zh. Eksp. Teor. Fiz. **72**, 970 (1977) [Sov. Phys. JETP **45**, 507 (1977)].
[35]N. G. Basov, A. A. Erokhin, Yu. A. Zakharenkov, N. N. Zorev, A. A. Kologrivov, O. N. Krokhin, A. A. A. Rupasov, G. V. Sklizkov, and A. S. Shikanov, Pis'ma Zh. Eksp. Teor. Fiz. **26**, 581 (1977) [JETP Lett. **26**, 433 (1977)].
[36]Ya. B. Zel'dovich and Yu. P. Raĭzer, Fizika udarnykh voln i vysokotemperaturnykh gazodinamicheskikh yavlenii (Physics of Shock Waves and High-Temperature Gasdynamic Phenomena), Nauka, 1966 [Academic].
[37]E. K. Storm, H. G. Ahlstrom, and J. F. Holzrichter, Report,

presented to the European Conf. on Laser Inter. with Matter, Palaiseau, France, LLL UCRL-78729, 1976. E. K. Storm, H. G. Ahlstrom, and M. J. Boyle, *et al.*, Laser Fusion Experiments, LLL, Preprint UCRL-78581, Rev. 1, 1976.
[38]M. H. Key, R. G. Evans, and D. J. Nicholas *et al.*, Implosion and compression of Gas Filled Microballoons, IV, 9 presented at the Eleventh European Conf. on Laser Inter. with Matter, Oxford, Sept. 1977, Preprint RL-77-122/B, Rutherford Laboratory, Chilton, Didcot, Oxon, OX 110QX.

Translated by J. G. Adashko